A beamline zero-degree spectrometer for measurements of projectile fragment distributions

G. A. Souliotis and D. J. Morrissey
National Superconducting Cyclotron Laboratory and Department of Chemistry, Michigan State University, East Lansing, Michigan 48824

B. M. Sherrill
National Superconducting Cyclotron Laboratory, Michigan State University, East Lansing, Michigan 48824

(Received 30 July 1990; accepted for publication 3 October 1990)

A technique for using a section of a beamline as a zero-degree spectrometer is described. The beamline magnets of the K1200 cyclotron at NSCL were operated as a zero-degree medium acceptance spectrometer to measure projectile fragment distributions. Projectile fragments were produced in a fragmentation target at the exit of the cyclotron and detected at the end of the beamline with a detector array consisting of two position-sensitive detectors and a $\Delta E - E$ telescope. Energy loss, position and angle at the focal plane and time of flight were measured for the isotopes produced. A procedure was developed to calculate the reaction angle and the momentum of the isotopes from the measured quantities. Typical examples of momentum and angular distributions of projectile fragments from a ^{14}N beam at 75 MeV/u with Al and Ta targets at and near 0° are shown.

I. INTRODUCTION

Projectile fragmentation is a very important mechanism for the production of nuclei far from stability. The exotic nuclei produced in this way can be separated and used as secondary (radioactive) beams, allowing the possibility of a new class of experiments to study nuclear structure and nuclear reaction mechanisms. The technique of converting a primary beam into a secondary radioactive beam by projectile fragmentation has been succesfully used at LBL,[1] GANIL,[2] and RIKEN[3] and similar devices are in the final construction stages for other labs (e.g., GSI[4]). At the National Superconducting Cyclotron Laboratory (NSCL), this technique is going to be realized by using a beam analysis device, the A1200.[5]

Projectile fragments are produced in peripheral collisions at intermediate and high energies. At high energies, above 200 MeV/u, there is a rather complete and systematic data set of the fragmentation distributions that have been successfully described by several models. In general, these models are based on the idea of a two-step process consisting of a fast collision step and a slow de-excitation one. At intermediate energies, from 50 to 200 MeV/u, there are only a few scattered measurements and no parametrization of the cross sections or understanding of the reaction mechanisms. In order to understand the reaction mechanisms of peripheral collisions at intermediate energies and obtain parametrizations of their distributions, refined measurements around 0° are necessary (since the projectile-like isotopes are produced in a narrow cone about 0°). Such systematic data and parametrizations, apart from a nuclear reaction standpoint, will improve our predictive power to choose the proper energy and beam-target combinations to produce a desired radioactive beam.

Measurements of reaction products at 0° are difficult in general, because of the presence of the primary beam and require the use of magnetic spectrometers. In this article we discuss a technique where, instead of a usual spectrometer, a section of a beamline containing one bending element was used for 0° measurements. We describe an experiment that we performed at NSCL in which the interim beamline[6] from the K1200 cyclotron to a 92-inch diameter cylindrical scattering chamber[7] was operated as a 0° spectrometer. Specifically, in this article, after a description of the beamline, its characteristics, and the detector system used, we discuss the measurements we performed with this system, the procedures we developed for the analysis of the data, and we show several representative results of projectile fragment distributions obtained from these data. Finally, in the Appendix, we include a derivation of the equations developed for the present study. Such techniques could be implemented at any laboratory with modest bending magnets in the beam transport system.

II. DESCRIPTION OF THE SPECTROMETER AND THE DETECTORS

The interim K1200 beamline consisted of four superconducting magnets (Fig. 1), which are a quadrudope singlet, a quadrupole doublet, a ±16° bending dipole magnet, and a quadrupole doublet. The details of these magnets have been described previously.[8] For the present study, we operated the two quadrupole doublets and the bending magnet as a 0° spectrometer (the quadrupole singlet was turned off). The characteristics of the magnetic elements of the spectrometer are summarized in Table I.

Projectile fragments, produced in a fragmentation target placed 40 cm after the exit of the K1200 cyclotron, traveled through the device and were focused and detected inside the 92-in. scattering chamber. The detection system for the present work was mounted on the movable radial arm of the chamber and consisted of two position counters

 0034-6748/91/020342-08$02.00

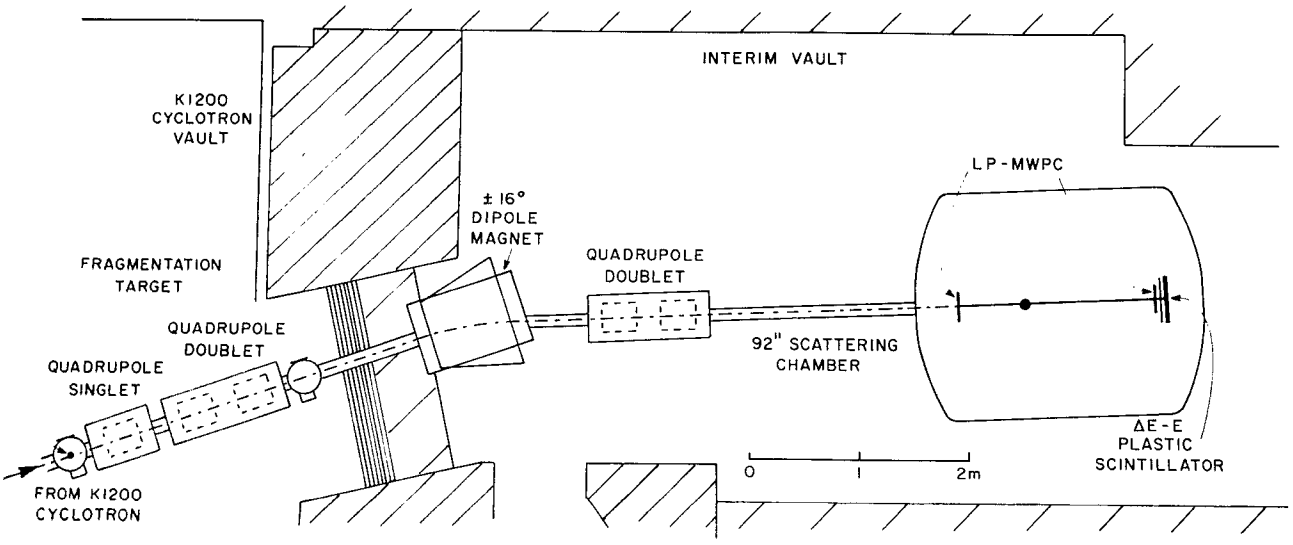

FIG. 1. Schematic layout of the beamline spectrometer.

and a $\Delta E - E$ plastic scintillator telescope. The first position counter was placed near the entrance to the 92-in. scattering chamber and the second counter 1.8 m further downstream. Both position counters were low pressure multiwire proportional counters (LP-MWPCs) of Breskin type.[9] From these detectors, a position signal is obtained by a delay-line readout of the electric charge induced on two layers of interleaved cathode strips. The time difference between the signals from the two ends of the delay line is measured and is proportional to position along the counter. The position measurement from the front counter contained information on the rigidity, whereas the difference between the position measurements of the two counters contained information on the scattering angle of a particle. Section V describes in detail how the rigidity and the scattering angle were obtained from the measured position and angle. The $\Delta E - E$ telescope, mounted behind the back position detector, consisted of a thin (3 mm) fast plastic scintillator for energy loss measurement and a thick (5 cm) plastic scintillator as a stopping detector. Each scintillator was viewed by a photomultiplier tube (PMT) on each end (left or right). A ΔE parameter was calculated event-by-event by taking the square root of the product of the left and right PMT signals of the ΔE scintillator. Due to light attenuation by self-absorption in the plastic scintillator, each PMT signal is exponentially dependent on the position of a particle along the scintillator. The product of the two signals is position independent and its square root proportional to ΔE (whereas the logarithm of the ratio of these signals is linearly related to position). The atomic number Z of the particles was obtained from the ΔE parameter, since $\Delta E \propto Z^2/v^2$, where v is the velocity of the particles.

TABLE I. Characteristics of the spectrometer and its elements.

Quadrupoles	
Effective length	43.0 cm
Pole-tip radius	5.08 cm
Max. magnetic field at pole tip	15 kG
Electric current at max. field	14 A
Distance between quads in a doublet	16.7 cm
Dipole	
Mean deflection angle	16.4°
Mean bending radius	3.08 m
Entrance face angle	0.0°
Exit face angle	16.4°
Effective length of central trajectory	0.882 m
Pole-gap width	5.0 cm
Maximum magnetic field	18 kG
Electric current at max. field	100 A
Distances between elements	
Target—first doublet entrance	1.187 m
First doublet exit—dipole entrance	1.677 m
Dipole exit—second doublet entrance	0.852 m
Second doublet exit—front LP-MWPC	2.662 m
Front LP-MWPC—back LP-MWPC	1.840 m

The back LP-MWPC had a low efficiency, so its position information was not used in the analysis of the data. Instead, a back position parameter was constructed from the logarithmic ratio of the two PMT signals of the ΔE scintillator. This position measurement was found to be consistent with the position measurement provided by the back LP-MWPC for highly ionizing particles and was combined with the front position parameter to provide a final angle parameter for the particles. The position resolution of both LP-MWPCs was 1 mm; the position resolution of the back position parameter obtained by the ΔE scintillator was 1.0 cm and the angle resolution obtained by the combination of this position parameter and the front position parameter was 6 mr. The fact that the angle measurement had to rely on the less accurate position values

TABLE II. Important parameters of the spectrometer.

Horizontal magnification	$(x\|x) = -0.63$
Dispersion at the front LP-MWPC	$(x\|\delta) = 0.65$ cm/%
Horiz. beam spot at the target (full width)	$\Delta x_0 = 6$ mm
Max. horiz. angular acceptance	$\Delta\theta_0 = 35$ mr
Max. vertical angular acceptance	$\Delta\phi_0 = 10$ mr
Max. solid angle	$\Delta\Omega = 0.35$ msr

First order TRANSPORT matrix elements

x	θ	y	ϕ	l	δ
−0.631 19	−0.073 02	0.000 00	0.000 00	0.000 00	0.649 14
18.661 88	0.574 52	0.000 00	0.000 00	0.000 00	0.611 10
0.000 00	0.000 00	1.606 86	0.809 37	0.000 00	0.000 00
0.000 00	0.000 00	1.537 34	1.396 69	0.000 00	0.000 00
1.249 98	0.041 76	0.000 00	0.000 00	1.000 00	−0.011 98
0.000 00	0.000 00	0.000 00	0.000 00	0.000 00	1.000 00

Second- and third-order matrix elements

$(x\|x\delta) = -1.18\times10^{-1}$	$(\theta\|x\delta) = -6.65\times10^{-1}$
$(x\|\theta\delta) = -4.53\times10^{-3}$	$(\theta\|\theta\delta) = -5.07\times10^{-2}$
$(x\|\theta^2) = -5.8\times10^{-5}$	$(\theta\|\theta^2) = -2.3\times10^{-4}$
$(x\|\delta^2) = 1.02\times10^{-3}$	$(\theta\|\delta^2) = 1.58\times10^{-2}$
$(x\|\theta\delta^2) = 2.78\times10^{-4}$	$(\theta\|\theta\delta^2) = 1.28\times10^{-3}$

Magnetic fields (in kG) for ^{14}N at 75 MeV/u

First quad	6.204	Third quad	1.701
Second quad	−3.667	Fourth quad	−0.041
Dipole	8.244		

from the plastic scintillator had a significant effect on the overall momentum resolution (see Sec. III).

Time of flight (TOF) was measured relative to the K1200 rf cycle. A start timing signal was obtained from the ΔE scintillator. A combination of TOF and position provided an A/q parameter, which was combined with the ΔE parameter in a two-dimensional histogram to provide particle identification. Due to multiple turn extraction from and the phase acceptance of the cyclotron, only limited TOF resolution (approximately 4 ns) was obtained, which hindered the particle identification for Zs higher than 6.

III. BEAM OPTICS CALCULATIONS

Beam optics calculations (up to third order), performed with the program TRANSPORT,[10] showed that a moderate acceptance solution was possible for this simple spectrometer, i.e., 35-mr horizontal and 10-mr vertical angular acceptances, and 8% momentum acceptance. The optical characteristics of the spectrometer, the first-order TRANSPORT matrix elements, and the important second- and third-order matrix elements at the front position counter are summarized in Table II. The TRANSPORT beam optics notation and units have been used in Table II and throughout this article. At the end of Table II, the field values of the magnets corresponding to setting the spectrometer for $^{14}N^{7+}$ at 75 MeV/u (which has a momentum-over-charge ratio P/q of 0.762 GeV/c/e) are given.

For the present system, there are no first-order correlations between the coordinates of the particle motion on the horizontal (bending) xz plane and the vertical (nonbending) yz plane. However, such correlations arise in second and higher orders. The TRANSPORT calculation showed that the second- and third-order correlations of horizontal and vertical coordinates are negligible for the relatively small vertical angular acceptance of 10 mr; in all cases, the contributions to the position and angle are less than 1 mm and 1 mr, respectively, and these contributions were neglected in the present study. Hence, only the correlations of the coordinates in the bending plane were taken into account when extracting the momentum and the scattering angle of a particle from the measured position and angle. Simple algebraic formulas and a calculation procedure were developed for this purpose and are described in Sec. V.

From the first-order TRANSPORT matrix, we see that a relatively small value of the horizontal magnification $(x|x)$ is achieved, but a considerable $(x|\theta)$ term is present at the front counter, which introduces a first-order correlation of final position with initial scattering angle. Consequently, a first-order horizontal focus was only approximately created at the front detector. The actual focal plane [where $(x|\theta)$ is zero] lies between the two detectors.

In any spectrometer with relatively large momentum and angular acceptance there will be large second-order aberrations [mainly due to the $(x|\theta\delta)$ term]. These can be corrected with sextupoles or by focal plane reconstruction. In the present study, we chose the later method. Consequences of this choice are that it is not necessary to have a first-order focus at a position-sensitive detector, but an accurate angular measurement is required.

Generally, it is desirable that the contributions of the second- and higher-order matrix elements at the focal plane should be small fractions (i.e., less than 0.1) of the displacement due to the dispersion. When one position counter is used at the exit of a spectrometer, it is necessary that this detector be placed at the position of the focal plane. However, if two position detectors are used (thus final position and angle of the particles can be measured, as in the present system), it is not necessary to place one of the detectors along the focal plane. In such a case, the position of the focal plane can, in principle, be reconstructed offline, provided that the angle measurement has sufficient accuracy.

For the present system, where reaction angle and momentum reconstruction are performed, an experimental uncertainty in the reaction angle of approximately 15 mr was obtained from the elastic scattering data. This value is consistent with a conservative estimate of 22 mr obtained from Eq. (A5), which takes into account the contribution from the final angle uncertainty and the beam-spot size (approximately 6 mm). Similarly, the experimental momentum resolution of approximately 2.0% can be mainly attributed to the reaction angle uncertainty combined with

the presence of the $(x|\,\theta)$ term. An estimate of the momentum resolution of approximately 2.0%, based on the beam optics, can be obtained from Eqs. (A3) and (A4). However, the momentum resolution of the system with only the front counter position, without scattering angle reconstruction, would be worse. Specifically, at the full horizontal angular acceptance of $\Delta\theta_0 = 35$ mr and momentum acceptance of $\Delta\delta = 8\%$ of the spectrometer, the effects of the $(x|\,\theta)$ and $(x|\,\theta\delta)$ terms to the image width would result in a momentum resolution of approximately 4.5%.

IV. EXPERIMENT

As a test of the beamline spectrometer, we measured the products from the reaction of a ^{14}N beam at 75 MeV/u with Al and Ta targets with thicknesses of 8 and 10 mg/cm^2, respectively. Data were collected for approximately 10 field settings in steps of 5%, covering the A/q region of 2.0 to 3.0. The magnetic field of the dipole was measured with an NMR magnetometer. The position and angle calibration of the detectors was performed in two independent ways, giving consistent results: first the radial arm (on which the detecting system was mounted) was rotated by a known angle and the change in position of the 0° elastically scattered beam particles was measured, and second, a slotted copper mask was inserted between the two counters and was irradiated with a dispersed primary beam.

V. DATA ANALYSIS AND RESULTS

In the present 0° spectrometer, the momentum and the scattering angle of a particle leaving the target are related to the measured position and angle at the front position counter. The calculations and the procedure that we have developed to extract these quantities from the data are described below.

We can write the magnetic rigidity $B\rho$ of a particle moving in the magnetic field of a dipole as[11]:

$$B\rho = 3.3356\,\frac{P}{q}, \tag{1}$$

where B is the magnetic field induction (in kG), ρ is the radius (in cm) of the trajectory of the particle in the dipole field, P is the momentum of the particle (in MeV/c), and q is its charge (in units of elementary charge). In the present experiment, the position of the undeflected beam particles at several charge states ($^{14}N^{7+}$ and $^{14}N^{6+}$) obtained at several different magnetic field settings, directly calibrated the curvature radius ρ versus position (Fig. 2) corresponding to a scattering angle θ_b with respect to the spectrometer optical axis at the target position [Fig. 3(a)]. This angle, made by the beam emerging from the accelerator, was found to be $\theta_b \cong 1°$. We had no control over this angle, since the spectrometer was fixed and there were no bending elements after the cyclotron and before the target. However, it was exploited to increase the observed reaction-angle range to 2°.

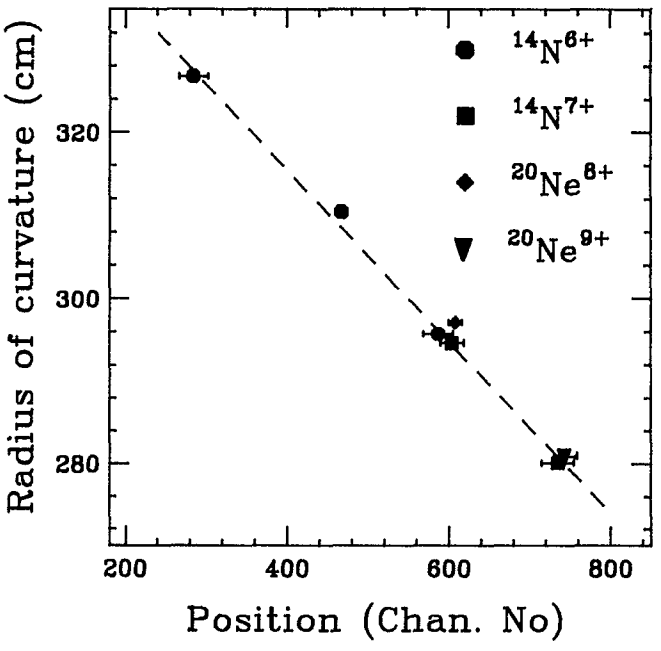

FIG. 2. Radius of curvature vs front counter position calibration. The error bars on the points have widths of 2σ. The widths of the peaks of the elastically scattered beam particles that arrive near the center of the front detector are mainly due to the magnification term $(x|\,x)$. The growth of the peak widths with increasing distance from the center of the detector is attributed to the momentum-dependent term $(x|\,x\delta)$.

The curvature radius–position calibration shown in Fig. 2 can be well described by a linear function:

$$\rho(\theta_b) = A_0(\theta_b) - A_1(\theta_b)X_{\rm FP}, \tag{2}$$

where $X_{\rm FP}$ is the position (in channel number) of a particle at the front position counter. Two additional calibration points, obtained in a subsequent experiment with a ^{20}Ne beam at 65 MeV/u, agree very well with the nitrogen data. So, for a particle emitted at an angle θ_b relative to the spectrometer axis, Eqs. (1) and (2) relate its momentum to the position on the front counter. But for angles θ_0 different from θ_b, the correlation of front counter position with angle θ_0 produced in the spectrometer, renders Eq. (2) inadequate. A θ_0 versus front counter position calibration would be necessary, which we were not able to obtain in the present experiment. There are at least two ways to perform this calibration; first by bending the beam before the target with an inflector magnet system and second, by inserting a slotted aperture at a certain distance after the target. In the present work, the calibration was obtained from a TRANSPORT calculation, which should be adequate, as the fields of the magnets and their positions along the beamline are well known. In order to take into account the angle dependence of the curvature radius, a relation similar to Eq. (2) was derived in which the coefficients A_0 and A_1 were expressed as functions of the angle θ_0 in first order. Specifically we can write, similar to Eq. (2):

$$\rho(\theta_0) = A_0(\theta_0) - A_1(\theta_0)X_{\rm FP}, \tag{3}$$

where now

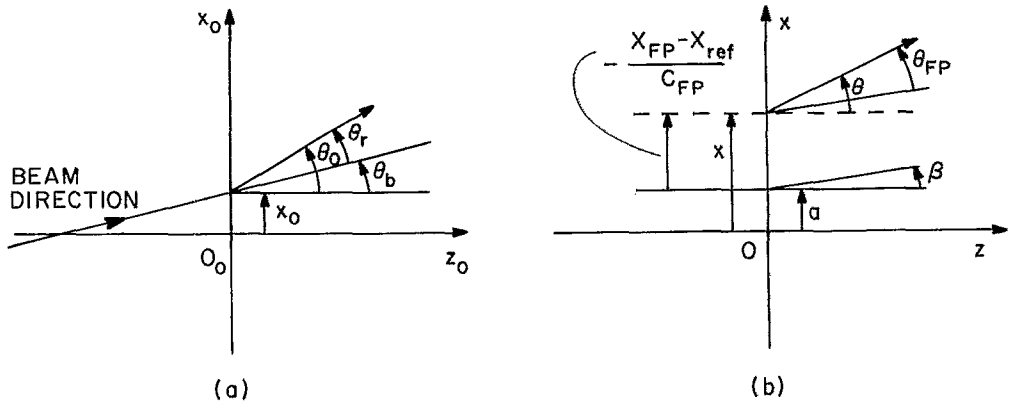

FIG. 3. Coordinate systems used in the calculations: (a) Initial coordinate system (at the target position). The beam strikes the target with an offset x_0 and an angle θ_b. Reaction products emerge from the target at angles θ_0 relative to the spectrometer axis (z axis). The interesting nuclear reaction angle is $\theta_r = \theta_0 - \theta_b$. (b) Final coordinate system (at the position of the front counter). In this system, α and β, respectively, are the position and angle coordinates of the 0° elastically scattered beam particles of one run that was chosen as reference; x, θ are the final position and angle coordinates, respectively, of a particle that entered the spectrometer with initial coordinates x_0, θ_0, and momentum deviation δ; the quantity $-(X_{FP} - X_{ref})/C_{FP}$ is the position of the particle relative to the reference position α and θ_{FP} is the angle of the particle relative to the reference angle β.

$$A_0(\theta_0) = A_0(\theta_b) - K_0(\theta_0 - \theta_b), \tag{4}$$

$$A_1(\theta_0) = A_1(\theta_b) - K_1(\theta_0 - \theta_b), \tag{5}$$

where the coefficients K_0 and K_1 are related to the calculated first-, second-, and third-order matrix elements with the following expressions (these equations are derived in the Appendix):

$$K_0 = \frac{\rho_0}{100(x|\,\delta)'}\left((x|\,\theta) + \frac{(x|\theta\,\delta)'}{(x|\,\delta)'}x_{off}\right), \tag{6}$$

$$K_1 = \frac{\rho_0}{100C_{FP}}\frac{(x|\,\theta\delta)'}{(x|\,\delta)'^2}, \tag{7}$$

where

$$(x|\,\theta\delta)' = (x|\,\theta\delta) + (x|\,\theta\delta^2)\delta, \tag{8}$$

$$(x|\,\delta)' = (x|\,\delta) + (x|\,x\delta)x_0, \tag{9}$$

$$x_{off} = (X_{ref}/C_{FP}) + \alpha - (x|\,x)x_0. \tag{10}$$

In these expressions we have $\delta = 100(\Delta P/P)$ the momentum deviation (in %) of the particle from the momentum of the central ray, ρ_0 the radius of curvature (in cm) of the central ray inside the dipole magnet, x_0 the x coordinate of the beam spot at the target position [Fig. 3(a)], C_{FP} the position calibration coefficient of the front position counter (in channels/cm), X_{ref} the position (in channel number) of the 0° elastically scattered beam particles of one run that was chosen as reference, and α the final position (in cm) of the reference beam particles relative to the optical axis of the spectrometer [Fig. 3(b)]. Terms including x_0 were taken to be zero, because the value of x_0 was not known.

One can see that Eqs. (4) and (5) are functions of the reaction angle $\theta_r = \theta_0 - \theta_b$, that is the angle of a particle leaving the target relative to the beam direction, which is, of course, the interesting nuclear reaction angle. This angle can be calculated by the formula:

$$\theta_r = \theta_0 - \theta_b = \frac{\theta_{FP} - [C_0(\theta_b) + C_1(\theta_b)\delta + C_2(\theta_b)\delta^2]}{(\theta|\,\theta) + (\theta|\,\theta\delta)\delta + (\theta|\,\theta\delta^2)\delta^2}, \tag{11}$$

where θ_{FP} is the angle (in mr) of a particle at the front position detector relative to the reference beam and $C_0(\theta_b)$, $C_1(\theta_b)$, $C_2(\theta_b)$ are the coefficients of a quadratic fit of the relation $\theta_{FP} = f(\delta)$ for the 0° elastically scattered beam particles (that is, for $\theta_0 = \theta_b$). So, the scattering angle of a given particle can be calculated according to Eq. (11) from its final angle θ_{FP} and its momentum deviation δ.

The δ dependence of the reaction angle θ_r and of the curvature radius $\rho(\theta_r)$ for a particle indicates that a successive approximation calculation has to be performed in order to obtain θ_r and $\rho(\theta_r)$ from the measured quantities X_{FP} and θ_{FP}. For this calculation, an initial value of δ for a particle was obtained from its position X_{FP} using Eq. (2) and the relation $\delta = 100(\rho - \rho_0)/\rho_0$. The convergence of this iteration is fast, i.e., in few steps.

Using these expressions and procedure, the curvature radius (thus the momentum) and the reaction angle of the particles were calculated on an event-by-event basis. The resolutions (FWHM) of the curvature radius and the reaction angle were approximately 2.0% and 15 mr, respectively.

As is standard in spectrometer measurements, an A/q parameter was constructed using the expression for the curvature radius and the measured TOF. Substituting the momentum $P = \gamma A m_p v$ in Eq. (1), we have

$$B\rho = 3.3356(\gamma A m_p v/q), \tag{12}$$

where γ is the relativistic factor $\gamma = [1 - (v^2/c^2)]^{-1/2}$, m_p is the nucleon mass (in MeV/c^2), and v is the velocity of the particle (in units of c, the speed of light). For the velocity of a particle we can write $v \propto L/(T - \mathrm{TOF})$, where L is the flight path length between the target and the timing detector, TOF is the measured time of flight (rela-

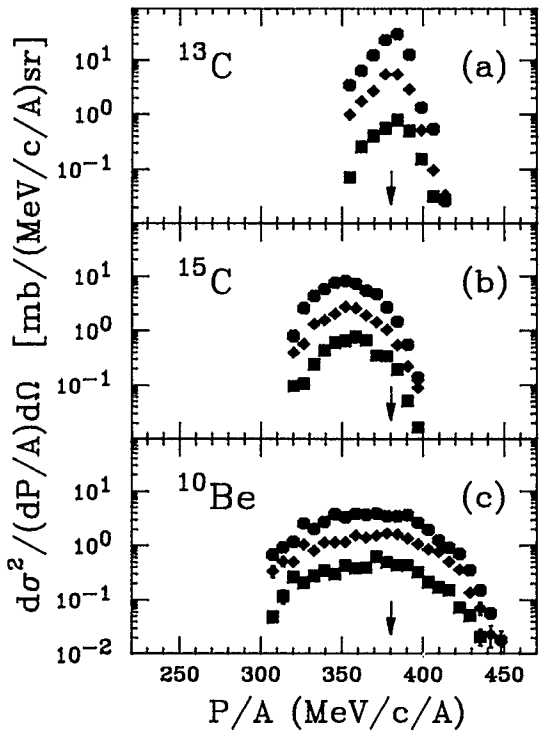

FIG. 4. Momentum distributions of some projectile-like isotopes produced from the reaction of ^{14}N at 75 MeV/u with Al target at 0° (closed points $\times 2$), 1° (diamonds $\times 1$), and 2° (squares $\div 2$). The beam momentum is indicated by an arrow.

tive to the rf cycle), and T is a constant (representing the number of rf periods elapsed between a given reaction at the target and the next beam pulse after the start signal for this event from the detector). Substituting this expression of v in Eq. (12), and solving for A/q we get:

$$\frac{A}{q} \propto B\rho \frac{T - \mathrm{TOF}}{L}, \tag{13}$$

from which the A/q parameter can be calculated also on an event-by-event basis.

Isotope separation and identification were performed using a two-dimensional histogram of ΔE vs A/q. In this histogram, the groups corresponding to the elastically scattered beam particles were used to calibrate the A/q axis. For each isotope, a θ_r vs P/q histogram was generated, θ_r cuts were made at 0°, 1°, 2°, (each with width of 1°) and the corresponding P/q spectra were constructed. Then, for each isotope, after normalization and appropriate combination of the spectra from different runs, a P/A spectrum at each of these angles was obtained. Finally, angular distributions were also constructed by integrating the P/A distributions at each angle.

As representative results of the present study, the momentum distributions of ^{13}C, ^{15}C, and ^{10}Be produced by the ^{14}N beam at 75 MeV/u on Al target and their angular distributions from Al and Ta targets are shown in Figs. 4 and 5, respectively. The error bars are statistical and are omitted when they are smaller than the plotting symbols. We conservatively estimate that a factor of approximately 2 accounts for the systematic errors primarily due to the uncertainty in the normalization of different runs with overlapping momenta (approximately ±20%) and to uncertainties in the beam current integration.

The present results exhibit the main characteristics of momentum and angular distributions of projectile-like isotopes produced at intermediate energies at and near 0°. Near-projectile fragments (one or two nucleons removed), like ^{13}C, have narrow momentum distributions peaked near (slightly lower than) the beam velocity. Their angular distributions show the effect of Coulomb deflection, since for the Al target they are steeper than those for the Ta target. If more nucleons are removed from the beam, the fragments, like ^{10}Be, have wider momentum distributions peaked again near the beam velocity. Transfer reaction products have also been observed in the experiment. The momentum distributions of these fragments are wider than those of similar few nucleon removal products (e.g., ^{15}C in contrast to ^{13}C) and interestingly they are peaked at considerably lower velocities than that of the beam. This novel feature provides hints of a rather complex mechanism of

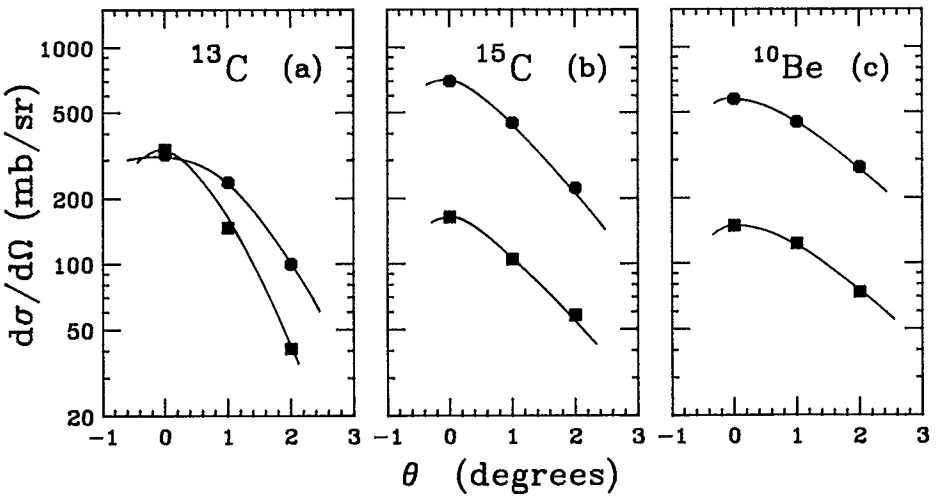

FIG. 5. Angular distributions of some projectile-like isotopes produced from the reaction of ^{14}N at 75 MeV/u with Al (squares) and Ta (closed points) targets. At each point, the angular bin has a full-width of 1°. The lines are just to guide the eye.

nucleon rearrangement between the projectile and the target and requires further systematic investigation.

ACKNOWLEDGMENTS

We wish to thank D. Mikolas and J. A. Winger for their help and suggestions during the course of the measurements.

APPENDIX: DERIVATION OF THE EXPRESSIONS FOR THE MOMENTUM AND THE REACTION ANGLE

The final position x of a particle at the front counter is related to the initial position x_0, initial angle θ_0 and δ with the expression[11] [see Figs. 3(a) and 3(b)]:

$$x=(x|\,x)x_0+(x|\,\theta)\theta_0+(x|\,\delta)\delta+(x|\,x\delta)x_0\delta+(x|\,\theta\delta)\theta_0\delta+(x|\,\delta^2)\delta^2+(x|\,\theta\delta^2)\theta_0\delta^2, \quad \text{(A1)}$$

where only the most important for the present system matrix elements are included (for example all y-dependent terms are dropped). After rearrangement, we can get the following equation for δ:

$$\delta=\frac{x-(x|\,x)x_0-(x|\,\theta)\theta_0}{(x|\,\delta)+(x|\,x\delta)x_0+(x|\,\theta\delta)\theta_0+(x|\,\delta^2)\delta+(x|\,\theta\delta^2)\theta_0\delta}.$$

Substituting $\delta = 100[(\rho/\rho_0) - 1]$ in the left side of the above equation, omitting the $(x|\,\delta^2)$ term (since it has a negligible contribution, see values in Table II), and using the abbreviated expressions:

$$(x|\,\theta\delta)'=(x|\,\theta\delta)+(x|\,\theta\delta^2)\delta,$$

$$(x|\,\delta)'=(x|\,\delta)+(x|\,x\delta)x_0,$$

we get

$$\rho=\rho_0+\frac{\rho_0}{100}\frac{x-(x|\,x)x_0-(x|\,\theta)\theta_0}{(x|\,\delta)'\{1+[(x|\,\theta\delta)'\theta_0/(x|\,\delta)']\}}.$$

Expanding the binomial in the denominator to first order in its argument (since it is small), we get:

$$\rho=\rho_0+\frac{\rho_0}{100(x|\,\delta)'}\left(1-\frac{(x|\,\theta\delta)'\theta_0}{(x|\,\delta)'}\right)[x-(x|\,x)x_0-(x|\,\theta)\theta_0].$$

Now, referring to Fig. 3(b), the position coordinate x (with respect to the coordinate system xOz in the horizontal plane), is related to the measured position $X_{\rm FP}$ (in channels) as

$$x=-\frac{X_{\rm FP}-X_{\rm ref}}{C_{\rm FP}}+\alpha,$$

in which the negative sign is due to the fact that the direction of increasing position as measured by the detector was taken to be opposite to that indicated by the coordinate system xOz. After substitution of this expression for x in the above equation and some algebraic manipulation, keeping terms up to first order in θ_0, we arrive at the relation:

$$\rho(\theta_0)=A_0(\theta_0)-A_1(\theta_0)X_{\rm FP},$$

where

$$A_0(\theta_0)=\left(\rho_0+\frac{\rho_0}{100(x|\,\delta)'}x_{\rm off}\right)-\frac{\rho_0}{100(x|\,\delta)'}\times\left((x|\,\theta)+\frac{(x|\,\theta\delta)'}{(x|\,\delta)'}x_{\rm off}\right)\theta_0$$

and

$$A_1(\theta_0)=\frac{\rho_0}{100(x|\,\delta)'C_{\rm FP}}\left(1-\frac{(x|\,\theta\delta)'}{(x|\,\delta)'}\theta_0\right)$$

with the definition:

$$x_{\rm off}=(X_{\rm ref}/C_{\rm FP})+\alpha-(x|\,x)x_0.$$

By writing the equations of $A_0(\theta_0)$ and $A_1(\theta_0)$ for $\theta_0 = \theta_b$ and subtracting the latter from the former, we finally get:

$$A_0(\theta_0)=A_0(\theta_b)-\frac{\rho_0}{100(x|\,\delta)'}\left((x|\,\theta)+\frac{(x|\,\theta\delta)'}{(x|\,\delta)'}x_{\rm off}\right)\times(\theta_0-\theta_b)$$

and

$$A_1(\theta_0)=A_1(\theta_b)-\frac{\rho_0}{100C_{\rm FP}}\frac{(x|\,\theta\delta)'}{(x|\,\delta)'^2}(\theta_0-\theta_b).$$

In order to derive the equation for the scattering angle θ_r we start from the expression that relates the final angle θ of a particle at the front counter with the initial coordinates x_0, θ_0, and δ:

$$\theta=(\theta|\,x)x_0+(\theta|\,\theta)\theta_0+(\theta|\,\delta)\delta+(\theta|\,x\delta)x_0\delta+(\theta|\,\theta\delta)\theta_0\delta+(\theta|\,\delta^2)\delta^2+(\theta|\,\theta\delta^2)\theta_0\delta^2. \quad \text{(A2)}$$

Referring again to Fig. 3(b), we can write $\theta = \theta_{\rm FP} + \beta$, where $\theta_{\rm FP}$ is the angle of a given particle with respect to the angle of the reference 0° elastically scattered beam particles and β is the angle of these arbitrarily chosen ref-

erence beam particles with respect to the optical axis of the spectrometer. Substituting this into Eq. (A2) and rearranging we get

$$\theta_{FP}=C_0(\theta_0)+C_1(\theta_0)\delta+C_2(\theta_0)\delta^2,$$

with:

$$C_0(\theta_0)=-\beta+(\theta|\,x)x_0+(\theta|\,\theta)\theta_0,$$

$$C_1(\theta_0)=(\theta|\,\delta)+(\theta|\,x\delta)x_0+(\theta|\,\theta\delta)\theta_0,$$

$$C_2(\theta_0)=(\theta|\,\delta^2)+(\theta|\,\theta\delta^2)\theta_0.$$

By rewriting each of these equations for $\theta_0=\theta_b$ and subtracting from the corresponding equation for θ_0, we find:

$$C_0(\theta_0)=C_0(\theta_b)+(\theta|\,\theta)(\theta_0-\theta_b),$$

$$C_1(\theta_0)=C_1(\theta_b)+(\theta|\,\theta\delta)(\theta_0-\theta_b),$$

$$C_2(\theta_0)=C_2(\theta_b)+(\theta|\,\theta\delta^2)(\theta_0-\theta_b).$$

Substituting these expressions into the equation for θ_{FP}, and solving for $\theta_r=\theta_0-\theta_b$, we get:

$$\theta_r=\frac{\theta_{FP}-[C_0(\theta_b)+C_1(\theta_b)\delta+C_2(\theta_b)\delta^2]}{(\theta|\,\theta)+(\theta|\,\theta\delta)\delta+(\theta|\,\theta\delta^2)\delta^2}.$$

The abberation-limited momentum resolution of the system is given by:

$$R_{ab}=\Delta x_{ab}/(x|\,\delta), \tag{A3}$$

where Δx_{ab} is the image size, which can be estimated to a first approximation, by an addition in quadrature of the contributions from the different aberrations. For the present system, for a given value of δ, Δx_{ab} can be estimated as:

$$\Delta x_{ab}=\{[(x|\,x)\Delta x_0]^2+[(x|\,x\delta)\Delta x_0\delta]^2+[(x|\,\theta)d\theta_0]^2+[(x|\,\theta\delta)d\theta_0\delta]^2\}^{1/2}. \tag{A4}$$

The scattering angle uncertainty $d\theta_0$ can be estimated, to a first approximation, as:

$$d\theta_0=\frac{1}{(\theta|\,\theta)}\{d\theta_{FP}^2+[(\theta|\,x)\Delta x_0]^2\}^{1/2}, \tag{A5}$$

where $d\theta_{FP}$ is the uncertainty in the measured final angle θ_{FP}.

Expressions (A4) and (A5) follow from Eqs. (A1) and (A2), respectively, where the most important terms are kept and a quadratic addition of the corresponding errors is performed.

[1] J. Alonso, Proceedings of the Workshop on Research with Radioactive Beams, Washington DC (1984), Lawrence Berkeley Laboratory Report No. 18187 (unpublished).

[2] R. Anne, D. Bazin, A. C. Mueller, J. C. Jacmart, and M. Langevin, Nucl. Instrum. Methods A **257**, 215 (1987).

[3] T. Kubo, M. Ishihara, N. Inabe, T. Nakamura, H. Okuno, K. Yoshida, S. Simoura, K. Asahi, H. Kumagai, and I. Tanihata, in *Proceedings of the 1st International Conference on Radioactive Nuclear Beams*, Oct. 1989, Berkeley, California, edited by W. D. Myers, J. M. Nitschke, and E. B. Norman (World Scientific, Singapore, 1990), p. 563.

[4] G. Münzenberg, H. Geissel, P. Armbruster, K. H. Behr, B. Blank, K. H. Burkard, H. G. Clerc, M. Chen, J. P. Dufour, B. Franczak, J. J. Gaimard, E. Hanelt, R. Kirchner, O. Klepper, B. Langenbeck, F. Nickel, K. Poppensieker, M. S. Pravikoff, E. Roeckl, D. Schardt, K. H. Schmidt, H. J. Schött, Th. Schwab, B. M. Sherrill, K. Sümmerer, and H. Wollnik, *ibid.*, p. 91.

[5] B. M. Sherrill, W. Benenson, D. Mikolas, D. J. Morrisey, J. A. Nolen, and J. A. Winger, *ibid.*, p. 72.

[6] B. M. Sherrill, N. Anantaraman, H. Blosser, R. Blue, S. Bricker, J. C. Dekamp, J. Easley, J. D. Johnson, H. Laumer, D. Lawton, F. Marti, L. Morris, J. A. Nolen, R. M. Ronninger, D. P. Sanderson, J. S. Winfield, and A. F. Zeller, National Superconducting Cyclotron Laboratory Annual Report 1987, p. 183 (unpublished).

[7] D. P. Sanderson, J. Nolen, R. Swanson, N. Mooney, and R. Blue, *ibid.*, p. 227.

[8] A. F. Zeller, R. T. Swanson, J. A. Nolen, D. Landry, M. J. Dubois, and J. C. Dekamp, in *Proceedings of the 9th International Conference on Magnet Technology* (1985), edited by C. Mazinucci and P. Weymuth (Swiss Institute for Nuclear Research, Zurich, 1985), p. 160 and J. C. Dekamp, C. T. Magsig, J. A. Nolen and A. F. Zeller, IEEE Trans. Mag. **MAG-23**, 524 (1987).

[9] A. Breskin, Nucl. Instrum. Methods **196**, 11 (1982).

[10] D. C. Carey, Fermi National Accelerator Laboratory Technical Manual TM-1546, 1988 (unpublished).

[11] D. C. Carey, *The Optics of Charged Particle Beams* (Harwood Academic, Chuz, Switzerland, 1987).